Published in final edited form as:
Structure. 2010 May 12; 18(5): 638–648. doi:10.1016/j.str.2010.02.009.

Structure and Mechanism of Receptor Sharing by the IL-10R2 Common Chain

Sung-il Yoon[1,#], **Brandi C. Jones**[1], **Naomi J. Logsdon**[1], **Bethany D. Harris**[2], **Ashlesha Deshpande**[1], **Svetlana Radaeva**[3], **Brian A. Halloran**[1], **Bin Gao**[3], and **Mark R. Walter**[1,2,4]

[1]Department of Microbiology, University of Alabama at Birmingham, Birmingham, Alabama 35294

[2]Center for Biophysical Sciences and Engineering, University of Alabama at Birmingham, Birmingham, Alabama 35294

[3]Section on Liver Biology, Laboratory of Physiologic Studies, National Institute on Alcohol Abuse and Alcoholism, National Institutes of Health, Bethesda, MD 20892

Summary

IL-10R2 is a shared cell surface receptor required for the activation of five class 2 cytokines (IL-10, IL-22, IL-26, IL-28, and IL-29) that play critical roles in host defense. To define the molecular mechanisms that regulate its promiscuous binding, we have determined the crystal structure of the IL-10R2 ecto-domain at 2.14Å resolution. IL-10R2 residues required for binding were identified by alanine scanning and used to derive computational models of IL-10/IL-10R1/IL-10R2 and IL-22/IL-22R1/IL-10R2 ternary complexes. The models reveal a conserved binding epitope that is surrounded by two clefts that accommodate the structural and chemical diversity of the cytokines. These results provide a structural framework for interpreting IL-10R2 single nucleotide polymorphisms associated with human disease.

Introduction

IL-10R2 is a ubiquitously expressed and essential receptor chain for at least five IL-10 family cytokines that share ~10–20% sequence identity and distinct 3D structures (Donnelly et al., 2004; Walter, 2004). IL-10R2, first called CRF2–4, was originally discovered as an essential component of the IL-10 hetero-dimeric signaling complex formed between the IL-10R1 chain and IL-10R2 (Kotenko et al., 1997). Solution and cell binding studies have shown IL-10R1 exhibits high affinity (nM) for IL-10, whereas IL-10R2 chain affinity is very low (~mM) (Ding et al., 2000; Logsdon et al., 2002; Yoon et al., 2005; Yoon et al., 2006). IL-10 mediated assembly of the IL-10R1/IL-10R2 complex activates intracellular kinases, JAK1 and TYK2, which phosphorylate the intracellular domains of the receptor as

[4]Correspondence should be addressed to Mark R. Walter Phone (205) 934-9279, FAX (205) 934-0480 walter@uab.edu.
[#]Present address: Dept. of Molecular Biology, BCC-206 The Scripps Research Institute 10550 N. Torrey Pines Road, La Jolla, CA 92037

Accession Numbers
The coordinates for the structure of IL-10R2 have been deposited in the protein databank with the accession code 3LQM.

Supplemental Data
Supplemental data includes seven figures and four tables.

well as STAT3 (Moore et al., 2001). Subsequent studies have revealed IL-10R2 also forms IL-22R1/IL-10R2 (Kotenko et al., 2001; Xie et al., 2000), IL-20R1/IL-10R2 (Sheikh et al., 2004) and IL-28R1/IL-10R2 (Kotenko et al., 2003; Sheppard et al., 2003) heterodimers that are activated by IL-22, IL-26, and IL-28/ IL-29, respectively (Fig S1). Thus, IL-10R2 functions as a common signaling chain in the class 2 cytokine family as observed for gp130, IL-2γc, and GM-CSF βc chains in the class 1 cytokine family (Wang et al., 2009).

Cytokines that signal via IL-10R2 induce pleotropic activities that protect the host from over-exuberant immune responses and activate innate immunity programs in epithelial cells. IL-10 inhibits macrophage and dendritic cell function, prevents pro-inflammatory cytokine synthesis (e.g. TNF-α, IFN-γ, IL-12, IL-l), and blocks antigen presentation (Moore et al., 2001). As a result of its potent immunosuppressive functions, numerous pathogens, including HIV, evade host immune responses by increasing the production of cellular IL-10 (Blackburn and Wherry, 2007; Redpath et al., 2001). In addition, cytomegalovirus (CMV) and Epstein Barr virus (EBV) express their own virally encoded IL-10s (cmvIL-10 and ebvIL-10) that disrupt immune function (Slobedman et al., 2009). IL-22, produced by TH17 cells, induces epithelial cells to produce anti-microbial peptides (Liang et al., 2006) but also exhibits protective functions in the gut, lung, and liver (Radaeva et al., 2004; Zenewicz et al., 2007). IL-26 is also produced by TH17 cells, up-regulates pro-inflammatory genes in intestinal epithelial cells, and its expression is increased in active Chron's disease (Dambacher et al., 2009). Finally, IL-28 and IL-29 form the recently discovered type III interferon family (Kotenko et al., 2003; Sheppard et al., 2003). IL-28 and IL-29 exhibit potent antiviral activities in keratinocytes and dendritic cells and may play an important role in resolving hepatitis C infection (Ge et al., 2009).

The molecular basis, whereby IL-10R2 is able to form promiscuous receptor-ligand interactions is unknown. In addition, single nucleotide polymorphisms (SNPs) in the IL-10R2 extracellular domain are associated with hepatitis virus subtype B (HBV) persistence (Frodsham et al., 2006), early-onset colitis (Glocker et al., 2009), graft-versus-host disease related to transplant rejection (Lin et al., 2005; Sivula et al., 2009), and systemic sclerosis (Hikami et al., 2008); an autoimmune disease characterized by fibrosis of skin and other organs. Thus, structure-function studies on IL-10R2 may be useful in understanding SNPs that alter immune function and result in human disease.

To define the molecular basis for promiscuous binding to diverse cytokine complexes, the crystal structure of the soluble extracellular IL-10R2 chain (sIL-10R2) has been determined at 2.14Å resolution. A series of sIL-10R2 mutants were evaluated for binding to three different binary complexes (BCs, IL-22/sIL-22R1, cmvIL-10/sIL-10R1, hIL-10/sIL-10R1) using tri-molecular surface plasmon resonance (SPR) assays. The binding data provided input for computational docking studies to generate IL-10 and IL-22 ternary complex models. These studies reveal IL-10R2 uses a central common binding epitope, centered on $Y82^{IL\text{-}10R2}$, which is surrounded by two clefts that allow the IL-10R2 chain to scan the unique structures and chemistries of helices A and D on the cytokines. The studies reveal IL-10R2 shares a conserved recognition motif with gp130 and IL-2γc suggesting a common origin for the promiscuous class 1 and class 2 cytokine receptors. Despite these common features, sIL-10R2 forms structurally and energetically distinct contacts with IL-10/ sIL-10R1 and IL-22/sIL-22R1 BCs, which could assist in the prediction of IL-10R2 SNP function.

Results

Structure Determination

The sIL-10R2 chain crystallized in spacegroup P6 with 2 molecules (chain A and B) in the asymmetric unit (Fig S2). Crystals of sIL-10R2 were first obtained from protein expressed in insect cells where N-linked glycosylation sites $N49^{sIL\text{-}10R2}$, $N68^{sIL\text{-}10R2}$, $N102^{sIL\text{-}10R2}$ and $N161^{sIL\text{-}10R2}$, were mutated to glutamine (sIL-10R2-NQ). sIL-10R2-NQ binds to the IL-22/sIL-22R1 complex with twofold weaker affinity (K_d = 14μM) than glycosylated sIL-10R2 (K_d = 7μM) expressed in insect cells. For phasing, sIL-10R2, containing a $C106^{sIL\text{-}10R2}$ to Ser mutation, was expressed in *E. coli* as a seleno-methionine labeled protein and refolded from insoluble inclusion bodies. Larger crystals, used for data collection and refinement (crystal 2, Table 1), were obtained with a sIL-10R2 double mutant ($C106S^{sIL\text{-}10R2}$/$S126C^{sIL\text{-}10R2}$). The structure of was solved by SAD phasing and refined at 2.14Å resolution to R_{cryst} and R_{free} values of 21.7% and 23.7%, respectively (Table 1). Electron density was observed for residues 20–220 in chain A and 20–215 in chain B. sIL-10R2 residue numbering is based on the sequence found in the Uniprot database code Q08334.

Structure of sIL-10R2 and comparison with high affinity R1 chains

The overall structure of sIL-10R2 is similar to the previously determined structures of sIL-10R1 and sIL-22R1 (Bleicher et al., 2008; Jones et al., 2008; Josephson et al., 2001). sIL-10R2 consists of two fibronectin type III domains (FBNIII) each comprising 7 β-strands (Fig 1A). The N-terminal domain, D1, and C-terminal domain, D2, adopt an inter-domain angle of approximately 95° (elbow angle, Fig S2) which is similar to the high affinity sIL-10R1 and sIL-22R1 chains (Figs 1B, S2). As seen in Figure 1B, the overall domain orientations of sIL-10R2 are closer to sIL-22R1 than sIL-10R1.

The sIL-10R2 β-strands are connected by a series of loops (L2-L6), which are predicted to mediate ligand binding (Fig 1A, (Jones et al., 2008;Pletnev et al., 2005)). sIL-10R2 L2 and L5 loops exhibit large structural differences compared to L2 and L5 in the sIL-10R1 and sIL-22R1 chains (Figs 1B and 2). $L2^{sIL\text{-}10R2}$ adopts a β-hairpin structure that is 2 residues shorter than observed for the L2 loops in sIL-10R1 and IL-22R1. As a result, L2 residue $Y59^{sIL\text{-}10R2}$ cannot form the canonical high affinity “R1 like” interaction, which consists of tyrosine residues on the L2 loops of the R1 chains ($Y43^{sIL\text{-}10R1}$ and $Y60^{sIL\text{-}22R1}$) that insert into clefts formed by the AB loops of the cytokines in the IL-10/sIL-10R1 and IL-22/sIL-22R1 complexes (Fig 1D, (Bleicher et al., 2008;Jones et al., 2008;Josephson et al., 2001)). Thus, the conformation of sIL-10R2 L2 is consistent with the low affinity of the sIL-10R2 chain for its various binding partners.

The sIL-10R2 L5 loop forms a “thumb-like” structure that extends away from the rest of the molecule (Figs 1A and 2). Despite conformational differences at the tip of L5 in chains A and B due to crystal contacts, both L5 loops exhibit the same overall “thumb” structure (Fig S2). The novel conformations of the sIL-10R2 L2 hairpin and L5 thumb give rise to two distinct clefts (Fig 2). The first is formed between the L2 and L3 loops (L2/3 cleft) and the second is between L3 and L5 (L3/L5 cleft). In contrast to sIL-10R2, no clefts are found in the high affinity IL-10R1 chain, and only very small L2/L5 and L3/L5 clefts are observed in sIL-22R1 (Fig 2). Interestingly, IL-22R1 is also a shared receptor, which forms IL-22R1/IL-10R2 and IL-22R2/IL-20R2 heterodimers (Dumoutier et al., 2001). These structural features, combined with the presence of four surface exposed aromatic residues (Y59, Y82, Y140, and W143) on the L2, L3, and L5 loops (Fig 1C), suggest the clefts may play an important role in the promiscuous binding properties of sIL-10R2.

Identification of sIL-10R2 residues required for ternary complex formation

To identify sIL-10R2 residues required for promiscuous interactions with structurally and chemically diverse cytokines, a SPR assay was designed to evaluate the relative binding strength of sIL-10R2 alanine mutants to IL-10/sIL-10R1, cmvIL-10/sIL-10R1, and IL-22/IL-22R1 BCs (Figs 3, S3-S5). Of the 22 point mutants tested, only $Y82A^{sIL\text{-}10R2}$ displayed drastically reduced (~10–20% of sIL-10R2WT) binding to all 3 BCs (Fig 3). $Y59A^{sIL\text{-}10R2}$, located on the L2 loop, is the only other mutant that exhibited significantly reduced binding (~50% of WT) to all three complexes, but to a lesser extent than $Y82A^{sIL\text{-}10R2}$. Other mutants disrupted sIL-10R2 recognition of cmvIL-10/sIL-10R1 and hIL-10/sIL-10R1 complexes or IL-22/sIL-22R1 complexes, but not both. For example, $Y56A^{sIL\text{-}10R2}$ and $Y140A^{sIL\text{-}10R2}$ exhibit diminished binding (~20% of WT) to hIL-10/cmvIL-10 BCs, but had no impact on the recognition of IL-22/sIL-22R1. In contrast, $W143A^{IL\text{-}10R2}$, and to a lesser extent $E141^{IL\text{-}10R2}$, selectively disrupted IL-22/IL-22R1 recognition, but not hIL-10/cmvIL-10/sIL-10R1 binding. Together, these studies suggest L3 residue $Y82^{sIL\text{-}10R2}$ provides a centrally located common binding epitope, while different residues on L2 and L5 make distinct energetic contributions to binding in different binary complexes.

Six of the 22 sIL-10R2 mutants (Q119A, H128A, R130A, L132A, K135A, and Y173A), located on β-strands A, B and E of D2, targeted putative receptor-receptor contacts (Jones et al., 2008; Pletnev et al., 2005) between the D2 of the R1 chains and $D2^{sIL\text{-}10R2}$. $Y173A^{sIL\text{-}10R2}$ exhibited reduced binding (65% of WT) to IL-22/IL-22R1 but did not reduce binding to cmvIL-10/sIL-10R1 or hIL-10/sIL-10R1 complexes. The other five mutants had no impact on IL-10R2 binding to any binary complex (data not shown). Thus, from a limited analysis of D2 residues, we have not identified an essential sIL-10R2 residue (such as $Y82^{sIL\text{-}10R2}$ described above) involved in R1/R2 D2-D2 contacts. It is unclear if this is due to the limited number of residues analyzed or specific characteristics of the D2 binding interfaces themselves.

Generation of IL-10 and IL-22 ternary complexes by computational docking

To further understand the mechanisms which allow promiscuous IL-10R2 recognition, the mutagenesis data (Fig 3, Table S1, (Logsdon et al., 2004;Wolk et al., 2004;Wu et al., 2008;Yoon et al., 2006)) was used to guide computer-based docking of sIL-10R2 onto IL-22/sIL-22R1, cmvIL-10/sIL-10R1, and hIL-10/sIL-10R1 crystal structures (Jones et al., 2002;Jones et al., 2008;Josephson et al., 2001). Top ranked sIL-10R2 docking solutions, consistent with the mutagenesis data, were identified for IL-22/sIL-22R1 and cmvIL-10/sIL-10R1 complexes. However, sIL-10R2 docking to the hIL-10/sIL-10R1 complex was unsuccessful (Table S2, Fig S6).

IL-22/sIL-22R1/sIL-10R2 and cmvIL-10/sIL-10R1/sIL-10R2 ternary complexes (TC) are assembled from three major interaction surfaces labeled site 1, site 2, and site 3 (Figs 4 and 5, Tables S3, S4). Site 1 forms the high affinity cytokine/R1 contact surface, which is identical to what has been previously described for the IL-22/sIL-22R1 and cmvIL-10/sIL-10R1 binary complexes (Bleicher et al., 2008;Jones et al., 2002;Jones et al., 2008). The sIL-10R2 binding site 2 is centered on cytokine helices A and D, but also consists of receptor-receptor contacts in the cmvIL-10 TC (Figs 4, 5). Site 3 is formed from contacts between R1 and sIL-10R2 D2 domains near the C-termini of the receptors and in close proximity to the cell membrane (Figs 4, 5). While the overall structures of the IL-22 and cmvIL-10 TCs are similar, contacts in the site 2 and site 3 interfaces are considerably different as reflected in the sIL-10R2 binding data (Fig 3).

IL-22/sIL-22R1/sIL-10R2 complex

The IL-22/sIL-10R1/sIL-10R2 site 2 interface (910 Å^2) is formed exclusively between IL-22 and sIL-10R2. The major feature of site 2 is the protruding IL-22 “knob” surface formed by Y51^{IL-22}, which is sandwiched between Y82$^{sIL-10R2}$ and W143$^{sIL-10R2}$ in the sIL-10R2 L3/L5 cleft (Fig 4C). L5$^{sIL-10R2}$ does not contact sIL-22R1 in the ternary complex but is positioned adjacent to glycosylated helix A residue N54^{IL-22}. This creates an opening between sIL-22R1 and sIL-10R2 for the N54^{IL-22}-linked carbohydrate without disrupting complex formation (Fig 4A). N54^{IL-22} and R55^{IL-22} form interactions with L5$^{sIL-10R2}$ residues E141$^{sIL-10R2}$ and E139$^{sIL-10R2}$, respectively (Fig 4C, Table S3). Interactions made by Y82$^{sIL-10R2}$, W143$^{sIL-10R2}$, Y51^{IL-22}, and N54^{IL22} in the IL-22 TC provide an explanation for why these residues are critical for sIL-10R2 recognition of IL-22/sIL-22R1 (Fig 3). To further characterize the validity of model, IL-22 mutants described by Logsdon et al., were evaluated for their ability to activate STAT3 in human HepG2 liver cells, which express human IL-22R1 and IL-10R2 chains (Fig 4E). These studies reveal Y51^{IL-22}, N54^{IL-22}, R55^{IL-22}, and to a lesser degree E117^{IL-22}, are most important for activating IL-22 STAT3 activity in these cells. The biological activity data further supports the contacts observed in the IL-22 TC model (Fig 4), which includes mainchain and sidechain interactions between E117^{IL-22} and K81$^{sIL-10R2}$ in the L3/L5 cleft (Fig 4C).

The site 3 interface (315Å^2) occurs between β-strand C’ and the CC” loop on sIL-22R1 (residues 173–178), and β-strands B and E on sIL-10R2 (Fig 4D). The carbohydrate, attached to N172$^{sIL-22R1}$, is also important in site 3 because it stabilizes the CC’ loop for sIL-10R2 binding. When the carbohydrate attached to N172$^{sIL-22R1}$ is removed, crystallographic studies reveal CC’ loop residues 172–175, that contact sIL-10R2 in our model, become disordered (Bleicher et al., 2008). Although carbohydrate was not included in the docking experiments, it fits nicely between sIL-22R1 and sIL-10R2 D2 domains, suggesting it might also participate in sIL-22R1/sIL-10R2 site 3 interactions (Fig 4D). Y173$^{sIL-10R2}$, the only site 3 residue to significantly disrupt sIL-10R2 binding to IL-22/sIL-22R1, buries 89Å^2 of surface area and participates in two hydrogen bonds with E168$^{sIL-22R1}$ and H179$^{sIL-22R1}$. Other sIL-10R2 site 3 residues tested by mutagenesis (Q119A, H128A, R130A, L132A, K135A) form less extensive site 3 contacts and do not disrupt sIL-10R2 binding.

cmvIL-10/sIL-10R1/sIL-10R2 complex

The cmvIL-10 TC site 2 and site 3 interfaces bury 1,172Å^2 and 368Å^2 of accessible surface area, respectively (Fig 5). In contrast to the IL-22 TC, sIL-10R2 (L5$^{sIL-10R2}$) is positioned adjacent to the cmvIL-10/sIL-10R1 interface. As a result, receptor-receptor contacts in the cmvIL-10 TC are more than double (705 Å^2) the size of those in the IL-22 TC (315 Å^2). The increase is largely due to L5$^{sIL-10R2}$ residues Y140$^{sIL-10R2}$ and E141$^{sIL-10R2}$, which bury 121Å^2 and 78Å^2 of buried surface area, respectively, into the cmvIL-10 helix A / sIL-10R1 interface (Fig 5C). This structural feature provides an explanation for the importance of Y140$^{sIL-10R2}$ in cmvIL-10/sIL-10R1 and hIL-10/sIL-10R1 recognition, while it does not contribute to IL-22/sIL-22R1 binding (Fig 3).

There is no protruding knob, corresponding to Y51^{IL-22}, in cmvIL-10. Thus, few contacts are formed between the sIL-10R2 L3/L5 cleft and cmvIL-10. However, more extensive interactions are made between the sIL-10R2 L2/L3 cleft and cmvIL-10 helix D (Fig 5B). The L2/L3 cleft interactions are centered on Y56$^{sIL-10R2}$, which forms a hydrogen bond with the mainchain oxygen of T89$^{cmvIL-10}$. Consistent with the structural model, the mutagenesis data demonstrates Y56$^{sIL-10R2}$ is critical for binding to the cmvIL-10/sIL-10R1 complex, but not to IL-22/sIL-22R1 (Fig 3, Fig S3-S4). Despite differences in the interactions of Y56$^{sIL-10R2}$ and Y140$^{sIL-10R2}$, some contacts in the IL-22 and cmvIL-10 TCs are conserved.

First, Y82$^{sIL\text{-}10R2}$, located in the center of site 2, packs against R22$^{cmvIL\text{-}10}$, between helices A and D, in essentially the same position as observed in the IL-22TC (Fig 5C). In addition, energetically important binding residues Y59$^{sIL\text{-}10R2}$ and R60$^{sIL\text{-}10R2}$, located at the tip of L2$^{sIL\text{-}10R2}$, form similar contacts in both TCs. Y59$^{sIL\text{-}10R2}$ packs against helix D and R60$^{sIL\text{-}10R2}$ is positioned to form salt bridges with the conserved helix C residues E74$^{cmvIL\text{-}10}$ and E101$^{IL\text{-}22}$ (Figs 4B, 5B).

The amount of surface area buried in the cmvIL-10 TC site 3 (368 Å^2) is similar to the IL-22 TC (315Å^2). However, sIL-10R1 site 3 residues are donated from three β-strands (C, C', and E) rather than one (C') in the IL-22 TC. This is caused by the different D1/D2 inter-domain angle of sIL-10R1 compared to sIL-22R1 (Fig 1B, Fig S2). In contrast to the tightly clustered site 3 residues in the IL-22 TC, site 3 contacts in the cmvIL-10 TC are dispersed over the entire surface with no obvious energetically important interaction to stabilize the complex.

The crystal structure of the cmvIL-10/sIL-10R1 complex revealed cmvIL-10 forms a cysteine-linked dimer that binds two sIL-10R1 chains (Jones et al., 2002). As a result, the cell surface receptor complex presumably consists of two IL-10R1 and two IL-10R2 chains. A model of this complex was generated by superimposing 2 docking models (Fig 5A) onto the dimeric cmvIL-10/sIL-10R1 complex (Fig 5E). In the resulting complex, the twofold-related IL-10R1 and IL-10R2 chains are separated at their C-termini by 107Å and 122Å, respectively, and do not form contacts with one another (e.g. they are independent). The space between the two R1/R2 heterodimers is presumably occupied by the intracellular kinases JAK1 and TYK2, which associate with IL-10R1 and IL-10R2, respectively (Finbloom and Winestock, 1995). For each R1/R2 heterodimer, the spacing between the C-termini of the D2 domains is ~23Å (Table S2). Furthermore, the C-terminus of the IL-10R2 (last residue in D2, T194$^{sIL\text{-}10R2}$) is positioned ~9Å higher, relative to the putative position of the membrane, than the equivalent residue in sIL-10R1 (L205$^{sIL\text{-}10R1}$). Similar D2 asymmetries have been observed in the growth hormone receptor complex, and other ternary complexes (de Vos et al., 1992; Wang et al., 2009). The asymmetry is proposed to be induced by cytokine binding, which provides a structural mechanism by which JAK kinase activation may occur (Brown et al., 2005).

hIL-10/sIL-10R1/sIL-10R2 ternary complex

In contrast to docking studies performed with IL-22/sIL-22R1 and cmvIL-10/sIL-10R1, a high quality docking solution was not obtained using the hIL-10/sIL-10R1 complex. Additional computational studies were performed to try to determine why the docking failed. For example, was it due to subtle conformational differences in sIL-10R1s in the hIL-10/sIL-10R1 and cmvIL-10/sIL-10R1 BCs? To ask this question, sIL-10R1 from the cmvIL-10/sIL-10R1 structure was used to form a hybrid hIL-10/sIL-10R1cmv complex. However, a better docking solution was not obtained using this hybrid complex. In addition, docking studies were performed using an entire hIL-10 dimer and one sIL-10R1 chain to ensure the entire sIL-10R2 binding epitope was included in the experiment. However, these experiments were also unsuccessful.

Despite the inability to obtain a de novo docking solution, structural similarity between cmvIL-10/sIL-10R1 and hIL-10/sIL-10R1 complexes (.e.g. ½ of the dimeric complexes), and similar binding properties of sIL-10R2 mutants for both complexes (Fig 3), suggest sIL-10R2 contacts hIL-10/sIL-10R1 in essentially the same manner as observed in the cmvIL-10 TC. Based on these observations, a "best" hIL-10 TC model was generated by superposition of hIL-10/sIL-10R1 onto the cmvIL-10 TC. Contacts made by sIL-10R2 in this hIL-10 TC model support current and prior hIL-10 mutagenesis studies. In particular, the most important residue identified for the hIL-10/sIL-10R2 interaction is M22$^{hIL\text{-}10}$

(Yoon et al., 2006), which packs against similarly important Y82$^{sIL\text{-}10R2}$ in the hIL-10TC. Additional hIL-10 and sIL-10R2 residues important for sIL-10R2 binding that form putative hydrogen bonds in the hIL-10TC include N21$^{hIL\text{-}10}$/Trp143$^{sIL\text{-}10R2}$, R32$^{hIL\text{-}10}$/S78$^{sIL\text{-}10R2}$, and Ser93$^{hIL\text{-}10}$/Y56$^{sIL\text{-}10R2}$.

Discussion

This study was initiated to understand the molecular mechanisms that allow the sIL-10R2 common chain to promiscuously bind to at least five different class 2 cytokines, which induce diverse cellular activities. The questions we sought to address were: 1) what are the structural features of sIL-10R2 that facilitate promiscuous binding? 2) Does sIL-10R2 form energetically and structurally identical, or distinct, interactions when engaging different binding partners? In addition to determining the molecular basis for promiscuous low affinity protein-protein interactions (14–250μM), for which there is a paucity of literature, these studies also have implications for interpreting IL-10R2 SNPs which cause human disease. In particular, SNPs in sIL-10R2 result in numerous pathologies including early-onset colitis (Glocker et al., 2009) and persistent HBV infection (Frodsham et al., 2006). Several more IL-10R2 SNPs have been identified in patients with inflammatory bowel disease (personal communication, Christoph Klein, Hannover, de), which further argues for the need to understand the structure and mechanism of IL-10R2 binding.

High affinity interactions between hIL-10/sIL-10R1, cmvIL-10/sIL-10R1, and IL-22/sIL-22R1 binary complexes depend on a conserved L2 loop tyrosine, which inserts itself into a cleft between helices A and B on the respective cytokines (Fig 1D). This paradigm is reversed for sIL-10R2, which forms L2/L3 and L3/L5 clefts (Fig 2) that selectively recognize protruding surfaces on helix D$^{cmvIL\text{-}10}$, $^{hIL\text{-}10}$ and helix A$^{IL\text{-}22}$, respectively (Figs 4, 5). Thus, sIL-10R2 site 2 recognition is largely defined by the distinct interhelix angles, between helices A and D, found in the different cytokines (Presnell and Cohen, 1989;Walter, 2004), Figs 4A, 5A). Additional contacts are made by tyrosine, arginine, and glutamate residues located at the tips of L2$^{sIL\text{-}10R2}$ and L5$^{sIL\text{-}10R2}$.

While the sIL-10R2 clefts provide the ability to recognize distinct cytokine features, Y82$^{sIL\text{-}10R2}$ appears to be the common sIL-10R2 epitope required for interaction with each binary receptor complex, much like the conserved L2 tyrosine of sIL-10R1 and sIL-22R1 is highly conserved and required for high affinity IL-22 and IL-10 interactions (Fig 1D). Interestingly, prior structure-function studies on the shared receptors, gp130 and γc, has shown aromatic residues (F169^{gp130} and Y103$^{\gamma c}$) form conserved contacts in the center of the IL-6/gp130, IL-2/γc, and IL-4/γc interfaces (Wang et al., 2009). Superposition of the D1 domain of sIL-10R2, with gp130, and γc reveals L3 Y82$^{sIL\text{-}10R2}$ is structurally conserved with F169^{gp130} and Y103$^{\gamma c}$ (Fig 6A). Furthermore, superposition of IL-6 from the IL-6/IL-6R/gp130 structure and IL-22 from the IL-22/sIL-22R1/sIL-10R2 model, reveals Y82$^{sIL\text{-}10R2}$ and F169^{gp130} are separated by 4Å (Cα atoms) in their respective complexes (Fig 6B). This result provides additional independent data to confirm the IL-22 TC model (Fig 4), and suggests the structurally conserved L3 aromatic residues (Tyr or Phe) form the critical common binding epitope used by the shared cytokine receptors, gp130, IL-2γc, and IL-10R2, to recognize diverse cytokine surfaces. Mutation of F169^{gp130} and Y103$^{\gamma c}$ functionally disrupts receptor-ligand interactions and subsequent cell signaling (Kurth et al., 1999;Middleton et al., 1996). Together, these data suggest Y82$^{sIL\text{-}10R2}$ is critical for sIL-10R2 function and hints at a common origin of promiscuous shared cytokine receptors.

In addition, Olosz and Malek (Olosz and Malek, 2000) pointed out Y103$^{\gamma c}$ is structurally conserved with the erythropoietin receptor (EPOR) residue, F93. However, the position of F93^{EPOR} has diverged significantly from the tight cluster of common chain aromatic

residues shown in Figure 6A (Fig S7). Nonetheless, it is notable that $F93^{EPOR}$ is found in the interface of the EPO/EPOR complex (Syed et al., 1998) and in the interface of the EPOR dimer structure, which presumably mimics the unbound EPOR cell surface complex (Livnah et al., 1999). In contrast to IL-10R2, gp130, and γc, EPOR, as well as the growth hormone receptor (GHR), form homodimeric receptor complexes (e.g. 1:2 EPO/EPOR or GH/GHR, (de Vos et al., 1992; Syed et al., 1998)). GHR also contains a functionally critical aromatic residue in its L3 chain ($W104^{GHR}$, (Clackson and Wells, 1995)), but its position has diverged even further away from $Y82^{sIL\text{-}10R2}$ than $F93^{EPOR}$ (Fig S7). This suggests L3 aromatic residues are generally critical for recognition of diverse class 1 and class 2 cytokines. However, EPOR and GHR, which must form high and low affinity binding interfaces, presumably require greater structural diversity in the positions of their aromatic residues ($F93^{EPOR}$ and $W104^{GHR}$) than the specialized common chain receptors (IL-10R2, gp130, γc), which only form promiscuous low affinity contacts.

Since IL-10R2 activates multiple cytokine complexes, the cellular phenotype of an IL-10R2 SNP can be caused by disrupting the function of one or more cytokines. Thus, we sought to determine if sIL-10R2 mutants will have the same binding phenotype is each complex. Our studies found select sIL-10R2 residues ($Y56^{sIL\text{-}10R2}$, $Y140^{sIL\text{-}10R2}$, and $W143^{sIL\text{-}10R2}$) have distinct energetic functions in the IL-22 and cmvIL-10/hIL-10 TCs (Figs 3, S5). This result suggests specific sIL-10R2 SNPs could selectively disrupt IL-10 or IL-22 signaling and suggests caution should be applied in attributing biological outcomes to specific cytokines. Additional studies will be required to characterize how IL-26 and IL-28/IL-29 are recognized by IL-10R2.

The studies reported here have focused on sIL-10R2 residues directly involved in cytokine and R1 chain recognition. However, other mechanisms that disrupt IL-10R2 function are possible. For example, the $K47E^{sIL\text{-}10R2}$ SNP, which is associated with failure to clear HBV, has been shown to increase IL-10R2 expression levels on cells (Frodsham et al., 2006). Consistent with this interpretation, we found $E47^{sIL\text{-}10R2}$ and $K47^{sIL\text{-}10R2}$ had no impact on sIL-10R2 binding to IL-22/sIL-22R1 (data not shown). From a structural perspective, $K47^{sIL\text{-}10R2}$ is considered the preferred residue since it forms a salt bridge with $E96^{sIL\text{-}10R2}$, which would be disrupted when replaced with a glutamate residue (Fig 1E). How this mutation increases IL-10R2 surface expression remains unknown.

A key feature of IL-10R2 promiscuity is its very low affinity for the cellular cytokine complexes that it activates. This presents technical challenges that have, to date, prevented crystal structure analysis of the class 2 cytokine ternary complexes. To overcome this problem, we used computational docking studies to generate IL-22 and cmvIL-10 ternary complex models. Although not crystal structures, these models provide clear molecular explanations for how sIL-10R2 distinctly recognizes IL-22 and IL-10 binary complexes, which are consistent with experimental data. However, with the current docking parameters, we failed to generate an independent hIL-10 TC model. Interestingly, the success, or failure, of the docking experiments correlates with sIL-10R2 affinity for IL-22/sIL-22R1 (~14μM), cmvIL-10/sIL-10R1 (~80μM), and hIL-10/sIL-10R1 (~250μM) binary complexes (Logsdon et al., 2004; Yoon et al., 2005). This suggests successful sIL-10R2 docking requires a K_d of at least ~100μM using the current docking parameters and restraints.

In summary, our structural, biochemical, modeling, and activity data provide novel insights into the promiscuous binding of the IL-10R2 common chain. In particular, the studies demonstrate that despite being a shared weak-binding receptor, sIL-10R2 residues make distinct energetic and structural contributions to binding. This provides an molecular frame work to characterize additional IL-10R2 SNPs and might be used to design protein

therapeutics that restore one or more cytokine activities in patients with defective IL-10R2 signaling complexes.

Experimental Procedures

Expression and purification of sIL-10R2

For crystallization, sIL-10R2, with mutations N49Q, N68Q, N102Q, and N161Q (sIL-10R2NQ) and sIL-10R2NQ C106S/S126C, were expressed in insect cells as C-terminal his_6 fusion proteins. Mutagenesis was performed using QuikChange site-directed mutagenesis kit (Stratagene). sIL-10R2 was purified by nickel affinity chromatography and the his_6 tag was removed using Factor Xa protease (Novagen). The cleaved protein was further purified by anion exchange chromatography (Poros HQ/H 10/100) and gel filtration chromatography using Superdex 200 HR 10/30 columns.

For selenomethionine incorporation, pET-21a plasmid sIL-10R2NQ C106S was transformed into *E. coli* strain, B834 (DE3) (Novagen). Cells were grown using M9 SeMet high yield growth medium (Medicilon) at 37°C to OD_{600} = 0.6, and protein expression was induced with 1 mM IPTG for 8 hours. sIL-10R2NQ C106S inclusion bodies were purified and solubilized as previously described (Yoon and Walter, 2007). Solubilized sIL-10R2NQ C106S was refolded by rapid 10-fold dilution in refolding buffer containing 50 mM NaCl, 100 mM Tris-HCl (pH 8.0), 2.5 mM EDTA, 0.2 mM oxidized glutathione, 2 mM reduced glutathione, and 600 mM arginine and purified as described above.

Crystallization and data collection

sIL-10R2NQ C106S/S126C and SeMet-sIL-10R2NQ C106S proteins were concentrated to 10 mg/ml in 20 mM Tris pH 8.0, 150 mM NaCl and crystallized by hanging drop vapor diffusion methods with 0.95 M Li_2SO_4, 0.1 M Hepes, pH 7.5. Crystals were placed into cryoprotectant consisting of 20% glycerol, 1.4 M Li_2SO_4, and 0.1 M Hepes pH 7.5, and flash-frozen under a N_2 gas stream at 100° K. X-ray diffraction data were collected at the Advance Photon Source (SER-CAT ID22 beamline). All data were processed with HKL2000 (Otwinowski and Minor, 1997).

Structure determination and refinement

SAD diffraction data was collected on a single crystal of SeMet-sIL-10R2NQ C106S (Crystal 1, Table 1) and SeMet positions were identified using the program SOLVE (Terwilliger and Berendzen, 1999). The resulting phases were combined with structure factor amplitudes obtained from sIL-10R2NQ C106S/S126C crystal (Crystal 2, Table 1) and refined by solvent leveling/flipping using CNS version 1.1 (Abrahams and Leslie, 1996;Brunger et al., 1998). The sIL-10R2 model was built automatically using ArpWarp implemented in the CCP4i suite (Collaborative Computational Project 4, 1994;Lamzin and Wilson, 1993;Perrakis et al., 1997) and refinement was completed using CNS version 1.1 (Brunger et al., 1998).

SPR experiments

All sIL-10R2 proteins used for SPR studies (WT and mutants) contained the same NQ mutations as sIL-10R2-NQ used for structure determination. Each protein was expressed and purified as previously described (Logsdon et al., 2002). SPR data were obtained using a Biacore 2000 as previously described (Logsdon et al., 2004; Yoon et al., 2005; Yoon et al., 2006), except sIL-10R2, sIL-22R1, and sIL-10R1 were simultaneously injected over cytokines amine coupled to CM-5 sensor chips. IFN-τ4 (control surface), IL-22, cmvIL-10, and hIL-10 were coupled at final surface densities of 280–293RU, 220–274RU, 237–291RU, and 601–823RU, respectively. Maximal sIL-10R2 binding, in response units (RU),

was determined by subtracting a baseline response obtained by injecting 1μM sIL-10R1 and 500nM sIL-22R1 over the chip surface (Fig S3). Additional injections contained 1μM sIL-10R1, 500nM sIL-22R1, and 150μM sIL-10R2 or sIL-10R2 mutant (Supplemental Experimental Procedures, Figs S3-S4). An additional 25μM sIL-10R2 concentration was also tested with equivalent results (Fig S5). Absolute RUs were normalized to wild-type sIL-10R2. All sIL-10R2 mutants were tested at least twice. The error in the assay was determined by comparing 10 different wild-type sIL-10R2 experiments and also by evaluating replicates of the sIL-10R2 mutants. Both analyses revealed equivalent overall errors of 7%, 10%, and 23% for IL-22, cmvIL-10, and hIL-10 chip surfaces, respectively.

HADDOCK docking experiments

Docking studies were performed using the program HADDOCK (Dominguez et al., 2003) running on the UAB Cheaha computing grid (http://docs.uabgrid.uab.edu/wiki/Cheaha). Experiments consisted of rigid body docking of 1000 possible solutions evaluated using 180° sampling. The top 200 solutions were subjected to semi-flexible simulated annealing using CNS for atoms within 5Å of the interfaces (van Dijk et al., 2006). Finally, flexible explicit solvent refinement was performed to provide a final ranking of the solutions (van Dijk and Bonvin, 2006). Default energetic, refinement, and scoring parameters were used for all runs. Ambiguous interaction restraints (AIRs, Table S1) were chosen based on hIL-10 (Yoon et al., 2006), IL-22 (Logsdon et al., 2004; Wolk et al., 2004; Wu et al., 2008), and sIL-10R2 mutagenesis studies (Fig 3). Unambiguous restraints were applied to each Cα atom in the binary IL-22/sIL-22R1, hIL-10/sIL-10R1, and cmvIL-10/sIL-10R1 complexes resulting in 342 to 349 additional restraints. Solutions were clustered using an r.m.s.d. cut off of 7.5Å and evaluated graphically with PYMOL (DeLano, 2002). Buried surface areas were calculated with NACCESS (Hubbard and Thorton, 1993). Superpositions were performed by STAMP (Russell and Barton, 1992) as implemented in VMD (Humphrey et al., 1996).

Stat3 Activity Assay

Human hepatoma HepG2 cells (ATCC, Manassas, VA) were cultured in serum-free EMEM medium overnight followed by stimulation with IL-22 or IL-22 mutants (10 ng/ml) for 30 minutes. Cells were then washed with cold phosphate buffered saline, lysed, and protein extracts (30 μg) were prepared and used for Western blot analyses using anti-phospho-STAT3 (Tyr705) antibodies (Cell Signaling Technology, Beverly, MA).

Highlights

- The crystal structure of the IL-10R2 is distinct from IL-10R1 and IL-22R1 chains.
- IL-10R2 residues required for binding multiple cytokines have been identified.
- Docking studies provide structures of the promiscuous recognition paradigm.
- Class 1 and Class 2 receptor common chains exhibit conserved binding epitopes.

Supplementary Material

Refer to Web version on PubMed Central for supplementary material.

Acknowledgments

Use of the Advance Photon Source (SER-CAT, ID-22) was supported by the U.S. Department of Energy, Office of Science, Office of Basic Energy Sciences, under contract W-31-109-Eng-38. This work was funded by grants AI043700 and AI043700-08S1 from the NIH.

References

Abrahams JP, Leslie AG. Methods used in the structure determination of bovine mitochondrial F1 ATPase. Acta Crystallogr D Biol Crystallogr 1996;52:30–42. [PubMed: 15299723]

Blackburn SD, Wherry EJ. IL-10, T cell exhaustion and viral persistence. Trends Microbiol 2007;15:143–146. [PubMed: 17336072]

Bleicher L, de Moura PR, Watanabe L, Colau D, Dumoutier L, Renauld JC, Polikarpov I. Crystal structure of the IL-22/IL-22R1 complex and its implications for the IL-22 signaling mechanism. FEBS Lett 2008;582:2985–2992. [PubMed: 18675809]

Boulanger MJ, Chow DC, Brevnova EE, Garcia KC. Hexameric structure and assembly of the interleukin-6/IL-6 alpha-receptor/gp130 complex. Science 2003;300:2101–2104. [PubMed: 12829785]

Brown RJ, Adams JJ, Pelekanos RA, Wan Y, McKinstry WJ, Palethorpe K, Seeber RM, Monks TA, Eidne KA, Parker MW, Waters MJ. Model for growth hormone receptor activation based on subunit rotation within a receptor dimer. Nat Struct Mol Biol 2005;12:814–821. [PubMed: 16116438]

Brunger AT, Adams PD, Clore GM, DeLano WL, Gros P, Grosse-Kunstleve RW, Jiang JS, Kuszewski J, Nilges M, Pannu NS, et al. Crystallography & NMR system: A new software suite for macromolecular structure determination. Acta Crystallogr D Biol Crystallogr 1998;54(Pt 5):905–921. [PubMed: 9757107]

Clackson T, Wells JA. A hot spot of binding energy in a hormone-receptor interface. Science 1995;267:383–386. [PubMed: 7529940]

Collaborative Computational Project 4, C. The CCP4 suite: programs for protein crystallography. Acta Crystallogr D Biol Crystallogr 1994;50:760–763. [PubMed: 15299374]

Dambacher J, Beigel F, Zitzmann K, De Toni EN, Goke B, Diepolder HM, Auernhammer CJ, Brand S. The role of the novel Th17 cytokine IL-26 in intestinal inflammation. Gut 2009;58:1207–1217. [PubMed: 18483078]

de Vos AM, Ultsch M, Kossiakoff AA. Human growth hormone and extracellular domain of its receptor: crystal structure of the complex. Science 1992;255:306–312. [PubMed: 1549776]

DeLano, WL. The PyMOL Molecular Graphics System. San Carlos, CA, USA: DeLano Scientific; 2002. http://www.pymol.org

Ding Y, Qin L, Kotenko SV, Pestka S, Bromberg JS. A single amino acid determines the immunostimulatory activity of interleukin 10. J Exp Med 2000;191:213–224. [PubMed: 10637267]

Dominguez C, Boelens R, Bonvin AM. HADDOCK: a protein-protein docking approach based on biochemical or biophysical information. J Am Chem Soc 2003;125:1731–1737. [PubMed: 12580598]

Donnelly RP, Sheikh F, Kotenko SV, Dickensheets H. The expanded family of class II cytokines that share the IL-10 receptor-2 (IL-10R2) chain. J Leukoc Biol. 2004

Dumoutier L, Leemans C, Lejeune D, Kotenko SV, Renauld JC. Cutting edge: STAT activation by IL-19, IL-20 and mda-7 through IL-20 receptor complexes of two types. J Immunol 2001;167:3545–3549. [PubMed: 11564763]

Finbloom DS, Winestock KD. IL-10 induces the tyrosine phosphorylation of tyk2 and Jak1 and the differential assembly of STAT1 alpha and STAT3 complexes in human T cells and monocytes. J Immunol 1995;155:1079–1090. [PubMed: 7543512]

Frodsham AJ, Zhang L, Dumpis U, Taib NA, Best S, Durham A, Hennig BJ, Hellier S, Knapp S, Wright M, et al. Class II cytokine receptor gene cluster is a major locus for hepatitis B persistence. Proc Natl Acad Sci U S A 2006;103:9148–9153. [PubMed: 16757563]

Ge D, Fellay J, Thompson AJ, Simon JS, Shianna KV, Urban TJ, Heinzen EL, Qiu P, Bertelsen AH, Muir AJ, et al. Genetic variation in IL28B predicts hepatitis C treatment-induced viral clearance. Nature 2009;461:399–401. [PubMed: 19684573]

Glocker EO, Kotlarz D, Boztug K, Gertz EM, Schaffer AA, Noyan F, Perro M, Diestelhorst J, Allroth A, Murugan D, et al. Inflammatory bowel disease and mutations affecting the interleukin-10 receptor. N Engl J Med 2009;361:2033–2045. [PubMed: 19890111]

Hikami K, Ehara Y, Hasegawa M, Fujimoto M, Matsushita M, Oka T, Takehara K, Sato S, Tokunaga K, Tsuchiya N. Association of IL-10 receptor 2 (IL10RB) SNP with systemic sclerosis. Biochem Biophys Res Commun 2008;373:403–407. [PubMed: 18588853]

Hubbard, SJ.; Thorton, JM. Depart. Biochem., Molec. Biol. London: University College; 1993. NACCESS Computer Program.

Humphrey W, Dalke A, Schulten K. VMD: visual molecular dynamics. J Mol Graph 1996;14:33–38. 27–38. [PubMed: 8744570]

Jones BC, Logsdon NJ, Josephson K, Cook J, Barry PA, Walter MR. Crystal structure of human cytomegalovirus IL-10 bound to soluble human IL-10R1. Proc Natl Acad Sci U S A 2002;99:9404–9409. [PubMed: 12093920]

Jones BC, Logsdon NJ, Walter MR. Structure of IL-22 bound to its high-affinity IL-22R1 chain. Structure 2008;16:1333–1344. [PubMed: 18599299]

Josephson K, Logsdon NJ, Walter MR. Crystal structure of the IL-10/IL-10R1 complex reveals a shared receptor binding site. Immunity 2001;15:35–46. [PubMed: 11485736]

Kotenko SV, Gallagher G, Baurin VV, Lewis-Antes A, Shen M, Shah NK, Langer JA, Sheikh F, Dickensheets H, Donnelly RP. IFN-lambdas mediate antiviral protection through a distinct class II cytokine receptor complex. Nat Immunol 2003;4:69–77. [PubMed: 12483210]

Kotenko SV, Izotova LS, Mirochnitchenko OV, Esterova E, Dickensheets H, Donnelly RP, Pestka S. Identification of the functional interleukin-22 (IL-22) receptor complex: the IL-10R2 chain (IL-10Rbeta) is a common chain of both the IL-10 and IL-22 (IL-10-related T cell-derived inducible factor, IL-TIF) receptor complexes. J Biol Chem 2001;276:2725–2732. [PubMed: 11035029]

Kotenko SV, Krause CD, Izotova LS, Pollack BP, Wu W, Pestka S. Identification and functional characterization of a second chain of the interleukin-10 receptor complex. Embo J 1997;16:5894–5903. [PubMed: 9312047]

Kurth I, Horsten U, Pflanz S, Dahmen H, Kuster A, Grotzinger J, Heinrich PC, Muller-Newen G. Activation of the signal transducer glycoprotein 130 by both IL-6 and IL-11 requires two distinct binding epitopes. J Immunol 1999;162:1480–1487. [PubMed: 9973404]

Lamzin VS, Wilson KS. Automated refinement of protein models. Acta Crystallogr D Biol Crystallogr 1993;49:129–147. [PubMed: 15299554]

Liang SC, Tan XY, Luxenberg DP, Karim R, Dunussi-Joannopoulos K, Collins M, Fouser LA. Interleukin (IL)-22 and IL-17 are coexpressed by Th17 cells and cooperatively enhance expression of antimicrobial peptides. J Exp Med 2006;203:2271–2279. [PubMed: 16982811]

Lin MT, Storer B, Martin PJ, Tseng LH, Grogan B, Chen PJ, Zhao LP, Hansen JA. Genetic variation in the IL-10 pathway modulates severity of acute graft-versus-host disease following hematopoietic cell transplantation: synergism between IL-10 genotype of patient and IL-10 receptor beta genotype of donor. Blood 2005;106:3995–4001. [PubMed: 16109775]

Livnah O, Stura EA, Middleton SA, Johnson DL, Jolliffe LK, Wilson IA. Crystallographic evidence for preformed dimers of erythropoietin receptor before ligand activation. Science 1999;283:987–990. [PubMed: 9974392]

Logsdon NJ, Jones BC, Allman JC, Izotova L, Schwartz B, Pestka S, Walter MR. The IL-10R2 binding hot spot on IL-22 is located on the N-terminal helix and is dependent on N-linked glycosylation. J Mol Biol 2004;342:503–514. [PubMed: 15327950]

Logsdon NJ, Jones BC, Josephson K, Cook J, Walter MR. Comparison of interleukin-22 and interleukin-10 soluble receptor complexes. J Interferon Cytokine Res 2002;22:1099–1112. [PubMed: 12513909]

Middleton SA, Johnson DL, Jin R, McMahon FJ, Collins A, Tullai J, Gruninger RH, Jolliffe LK, Mulcahy LS. Identification of a critical ligand binding determinant of the human erythropoietin

receptor. Evidence for common ligand binding motifs in the cytokine receptor family. J Biol Chem 1996;271:14045–14054. [PubMed: 8662939]

Moore KW, de Waal Malefyt R, Coffman RL, O'Garra A. Interleukin-10 and the interleukin-10 receptor. Annu Rev Immunol 2001;19:683–765. [PubMed: 11244051]

Olosz F, Malek TR. Three loops of the common gamma chain ectodomain required for the binding of interleukin-2 and interleukin-7. J Biol Chem 2000;275:30100–30105. [PubMed: 10887198]

Otwinowski, Z.; Minor, W., editors. Processing x-ray diffraction data collected in oscillation mode. Pasadena, CA: Academic Press; 1997.

Perrakis A, Sixma TK, Wilson KS, Lamzin VS. wARP: improvement and extension of crystallographic phases by weighted averaging of multiple-refined dummy atomic models. Acta Crystallogr D Biol Crystallogr 1997;53:448–455. [PubMed: 15299911]

Pletnev S, Magracheva E, Wlodawer A, Zdanov A. A model of the ternary complex of interleukin-10 with its soluble receptors. BMC Struct Biol 2005;5:10. [PubMed: 15985167]

Presnell SR, Cohen FE. Topological distribution of four-alpha-helix bundles. Proc Natl Acad Sci U S A 1989;86:6592–6596. [PubMed: 2771946]

Radaeva S, Sun R, Pan HN, Hong F, Gao B. Interleukin 22 (IL-22) plays a protective role in T cell-mediated murine hepatitis: IL-22 is a survival factor for hepatocytes via STAT3 activation. Hepatology 2004;39:1332–1342. [PubMed: 15122762]

Redpath S, Ghazal P, Gascoigne NR. Hijacking and exploitation of IL-10 by intracellular pathogens. Trends Microbiol 2001;9:86–92. [PubMed: 11173248]

Russell RB, Barton GJ. Multiple protein sequence alignment from tertiary structure comparison: assignment of global and residue confidence levels. Proteins 1992;14:309–323. [PubMed: 1409577]

Sheikh F, Baurin VV, Lewis-Antes A, Shah NK, Smirnov SV, Anantha S, Dickensheets H, Dumoutier L, Renauld JC, Zdanov A, et al. Cutting edge: IL-26 signals through a novel receptor complex composed of IL-20 receptor 1 and IL-10 receptor 2. J Immunol 2004;172:2006–2010. [PubMed: 14764663]

Sheppard P, Kindsvogel W, Xu W, Henderson K, Schlutsmeyer S, Whitmore TE, Kuestner R, Garrigues U, Birks C, Roraback J, et al. IL-28, IL-29 and their class II cytokine receptor IL-28R. Nat Immunol 2003;4:63–68. [PubMed: 12469119]

Sivula J, Turpeinen H, Volin L, Partanen J. Association of IL-10 and IL-10Rbeta gene polymorphisms with graft-versus-host disease after haematopoietic stem cell transplantation from an HLA-identical sibling donor. BMC Immunol 2009;10:24. [PubMed: 19409109]

Slobedman B, Barry PA, Spencer JV, Avdic S, Abendroth A. Virus-encoded homologs of cellular interleukin-10 and their control of host immune function. J Virol 2009;83:9618–9629. [PubMed: 19640997]

Syed RS, Reid SW, Li C, Cheetham JC, Aoki KH, Liu B, Zhan H, Osslund TD, Chirino AJ, Zhang J, et al. Efficiency of signalling through cytokine receptors depends critically on receptor orientation. Nature 1998;395:511–516. [PubMed: 9774108]

Terwilliger TC, Berendzen J. Automated MAD and MIR structure solution. Acta Crystallogr D Biol Crystallogr 1999;55(Pt 4):849–861. [PubMed: 10089316]

van Dijk AD, Bonvin AM. Solvated docking: introducing water into the modelling of biomolecular complexes. Bioinformatics 2006;22:2340–2347. [PubMed: 16899489]

van Dijk M, van Dijk AD, Hsu V, Boelens R, Bonvin AM. Information-driven protein-DNA docking using HADDOCK: it is a matter of flexibility. Nucleic Acids Res 2006;34:3317–3325. [PubMed: 16820531]

Walter MR. Structural analysis of IL-10 and Type I interferon family members and their complexes with receptor. Adv Protein Chem 2004;68:171–223. [PubMed: 15500862]

Wang X, Lupardus P, Laporte SL, Garcia KC. Structural biology of shared cytokine receptors. Annu Rev Immunol 2009;27:29–60. [PubMed: 18817510]

Wolk K, Witte E, Reineke U, Witte K, Friedrich M, Sterry W, Asadullah K, Volk HD, Sabat R. Is there an interaction between interleukin-10 and interleukin-22? Genes Immun. 2004

Wu PW, Li J, Kodangattil SR, Luxenberg DP, Bennett F, Martino M, Collins M, Dunussi-Joannopoulos K, Gill DS, Wolfman NM, Fouser LA. IL-22R, IL-10R2, and IL-22BP binding sites

are topologically juxtaposed on adjacent and overlapping surfaces of IL-22. J Mol Biol 2008;382:1168–1183. [PubMed: 18675824]

Xie MH, Aggarwal S, Ho WH, Foster J, Zhang Z, Stinson J, Wood WI, Goddard AD, Gurney AL. Interleukin (IL)-22, a novel human cytokine that signals through the interferon receptor-related proteins CRF2-4 and IL-22R. J Biol Chem 2000;275:31335–31339. [PubMed: 10875937]

Yoon SI, Jones BC, Logsdon NJ, Walter MR. Same structure, different function crystal structure of the Epstein-Barr virus IL-10 bound to the soluble IL-10R1 chain. Structure 2005;13:551–564. [PubMed: 15837194]

Yoon SI, Logsdon NJ, Sheikh F, Donnelly RP, Walter MR. Conformational changes mediate interleukin-10 receptor 2 (IL-10R2) binding to IL-10 and assembly of the signaling complex. J Biol Chem 2006;281:35088–35096. [PubMed: 16982608]

Yoon SI, Walter MR. Identification and characterization of a +1 frameshift observed during the expression of Epstein-Barr virus IL-10 in Escherichia coli. Protein Expr Purif 2007;53:132–137. [PubMed: 17224278]

Zenewicz LA, Yancopoulos GD, Valenzuela DM, Murphy AJ, Karow M, Flavell RA. Interleukin-22 but not interleukin-17 provides protection to hepatocytes during acute liver inflammation. Immunity 2007;27:647–659. [PubMed: 17919941]

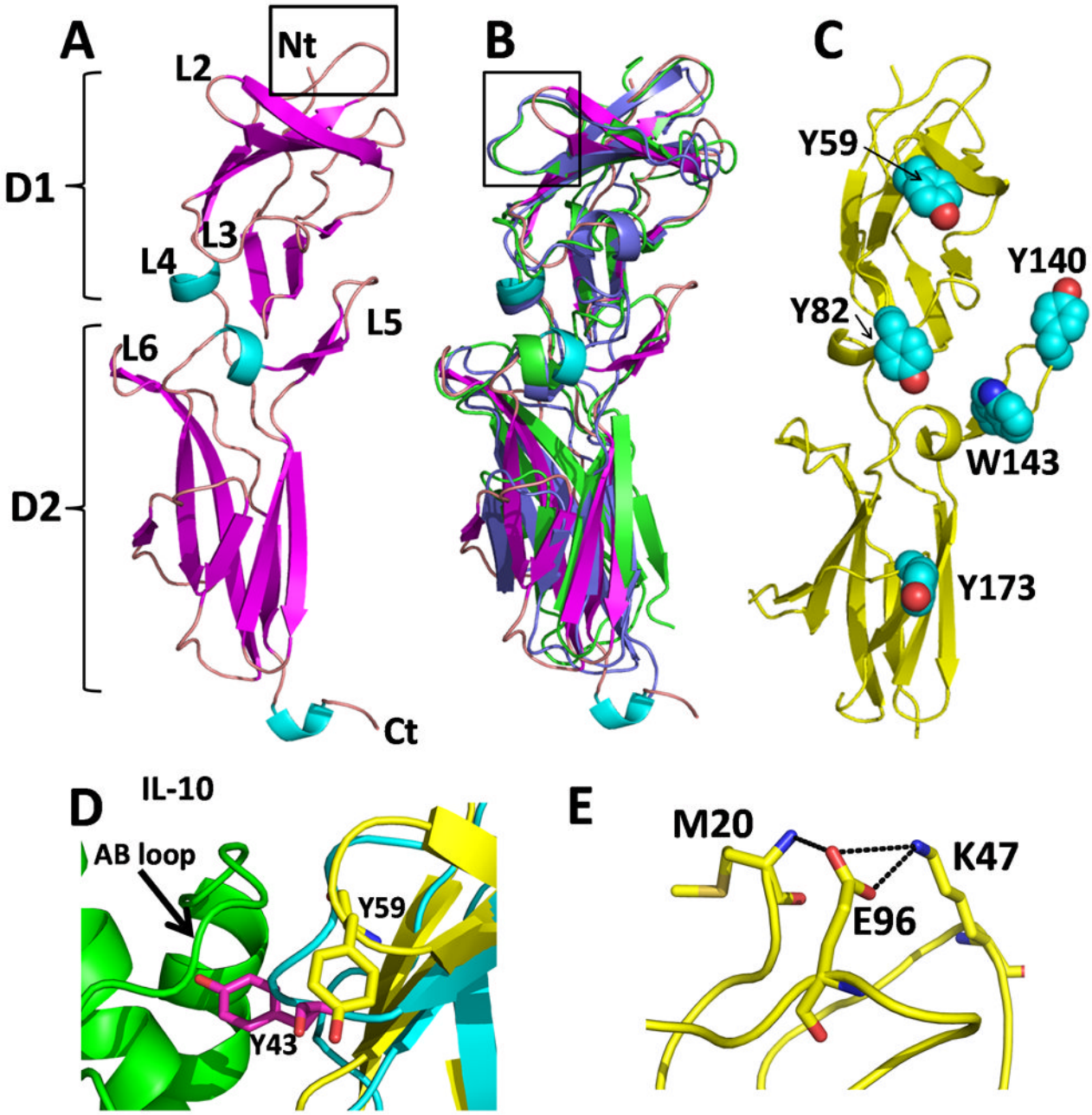

Figure 1. Structure of the sIL-10R2 chain

(**A**) Ribbon diagram of the sIL-10R2 chain colored by secondary structure with binding loops labeled. Box shows the location of Figure F. (**B**) Superposition of sIL-10R2 (colored as in A) with sIL-10R1 (green) and sIL-22R1 (purple). Box shows the location of Figure D. (**C**) Location of aromatic residues on sIL-10R2 on sIL-10R2. (**D**) Comparison of the high affinity site 1 interaction between sIL-10R1 $Y43^{sIL\text{-}10R1}$ and the AB loop of IL-10 (green) with the sIL-10R2 L2 loop and $Y59^{sIL\text{-}10R2}$ (yellow). (**E**) Interaction network for $K47^{sIL\text{-}10R2}$. Replacement of $K47^{sIL\text{-}10R2}$ with a glutamic acid is associated with persistent HBV infection (Frodsham et al., 2006).

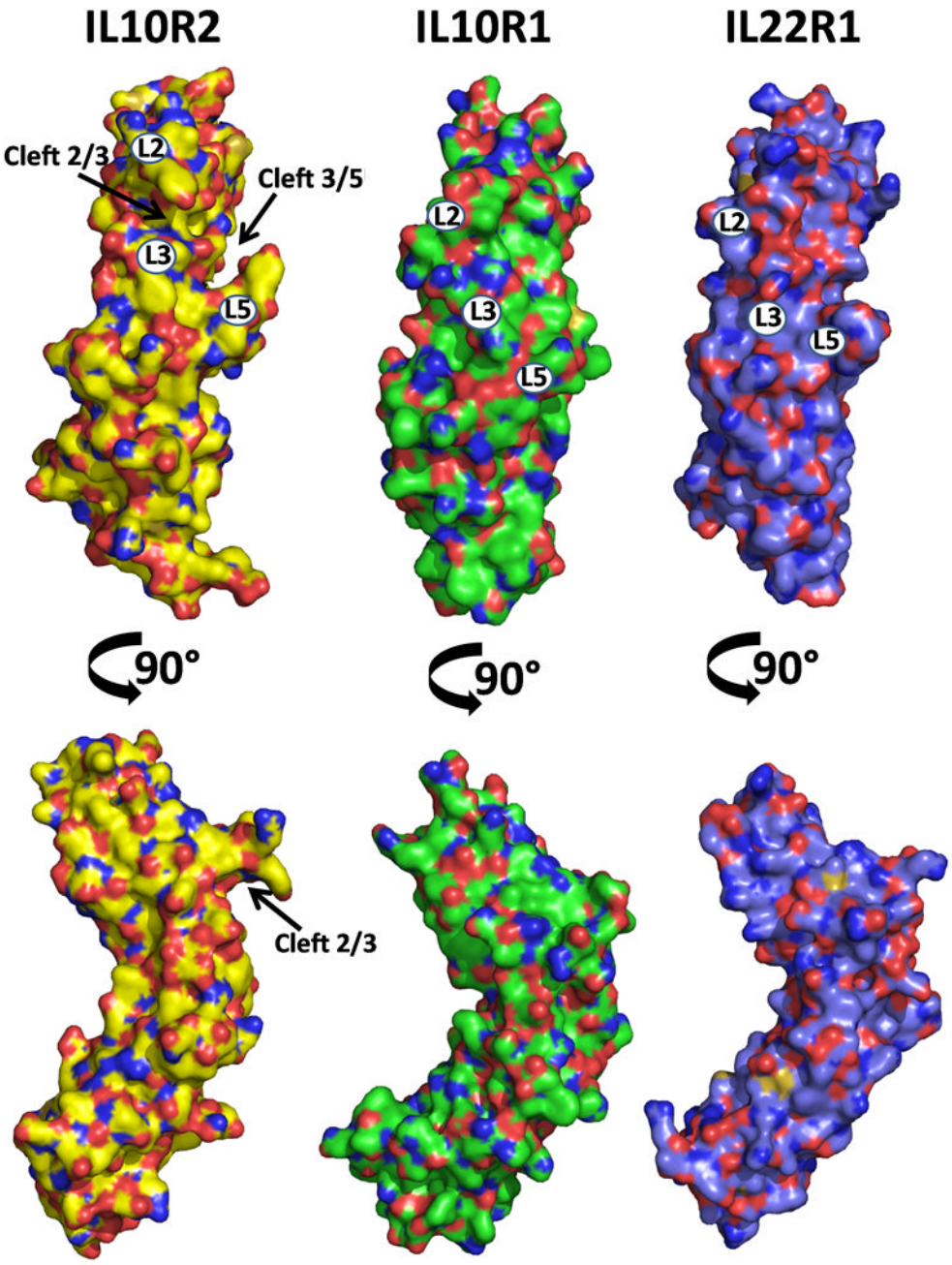

Figure 2. Unique clefts identified in sIL-10R2

The structures of sIL-10R2, sIL-10R1, and sIL-22R1 are shown as molecular surfaces. Images in the top row are orientated as found in Figure 1A. The surfaces are colored by atom type with oxygens red, nitrogens blue, and sulfur orange. Carbons are colored yellow, green, and purple in sIL-10R2, sIL-10R1, and sIL-22R1, respectively. Numbers on the surfaces correspond to loop positions.

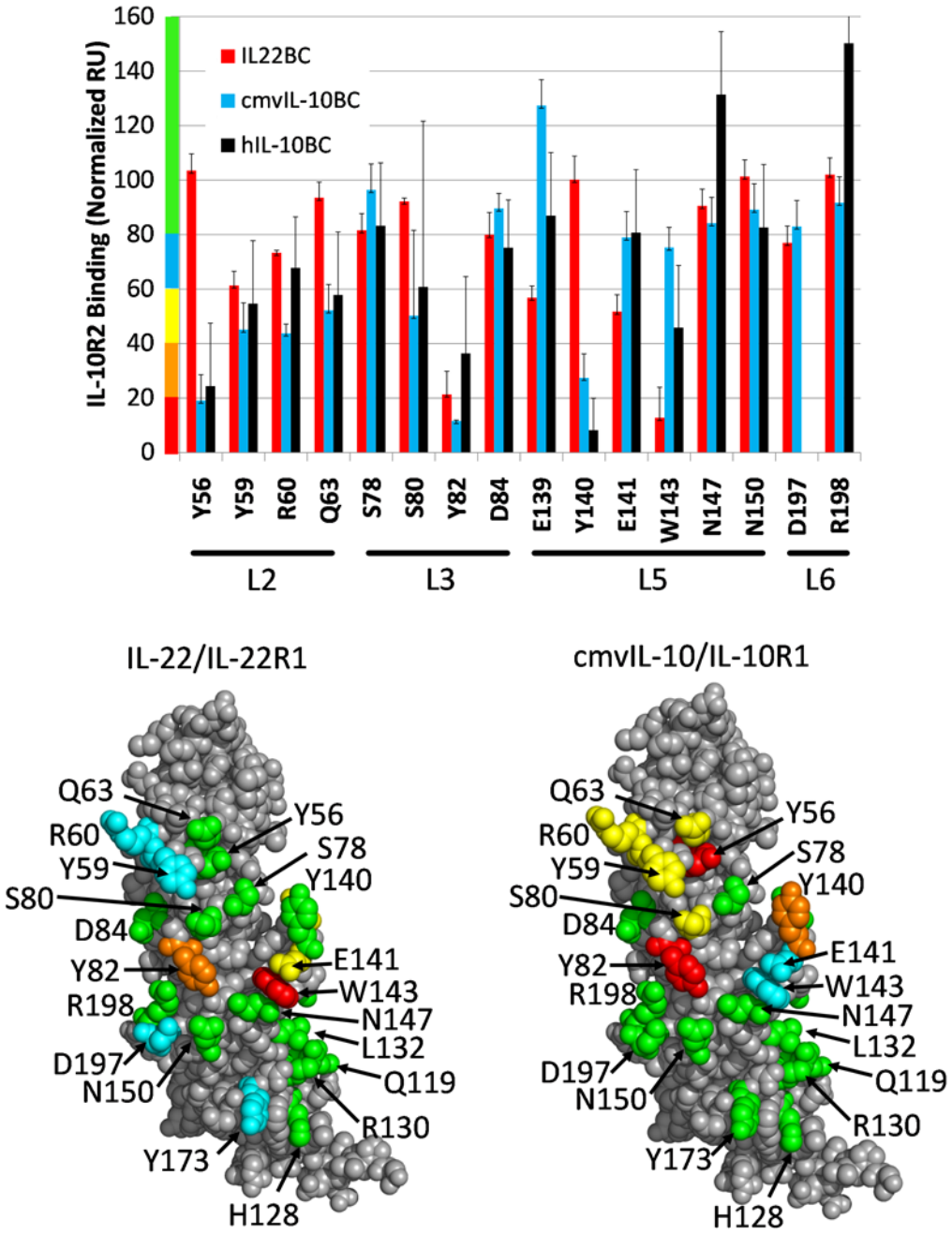

Figure 3. Binding analysis of sIL-10R2 alanine mutants by SPR

(A) Relative binding of sIL-10R2 alanine mutants to IL-22/IL-22R1 (red), cmvIL-10/IL-10R1 (cyan), and hIL-10/IL-10R1 (black) binary complexes. sIL-10R2 mutant binding is presented in normalized response units (RU) relative to wild-type sIL-10R2 binding at concentrations of 150μM. Results are expressed as the mean of multiple measurements ±standard deviation. Residues tested for binding to IL-22/sIL-22R1 **(B)** and cmvIL-10/IL-10R1 **(C)** are mapped onto sIL-10R2 surfaces and colored according to the y axis in Figure A (See also Figures S3-S5).

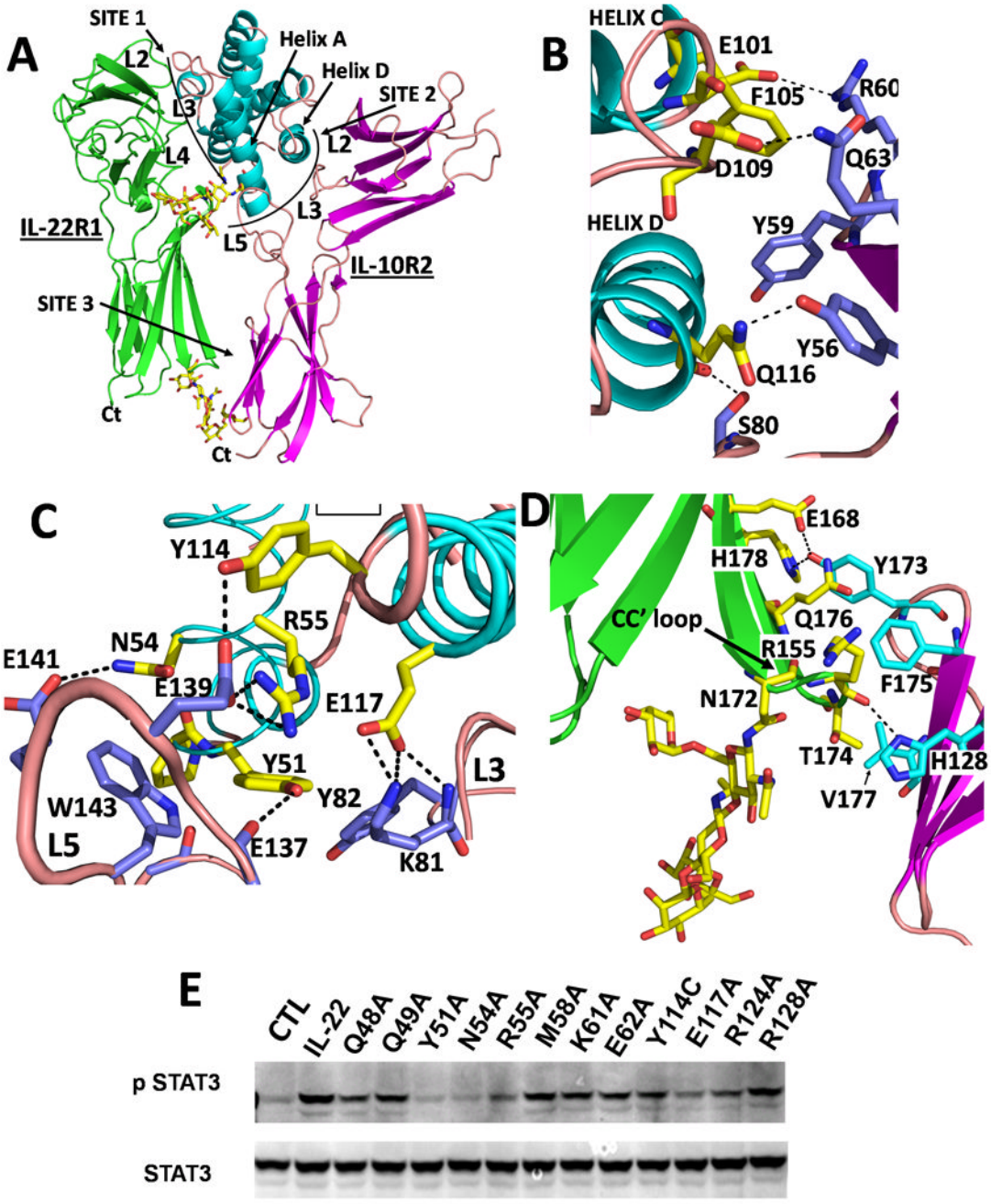

Figure 4. IL-22 Ternary complex

(A) Overall structure of the IL-22 ternary complex. **(B)** Site 2 interactions between helix D and the L2/L3 cleft. **(C)** Site 2 interactions between helix A and L3/L5 cleft. **(D)** Site 3 contacts **(E)** Anti-Phospho-STAT3 western blot from lysates prepared from HepG2 cells stimulated with IL-22 or IL-22 mutants (See Also Figure S6 and Tables S1-S4).

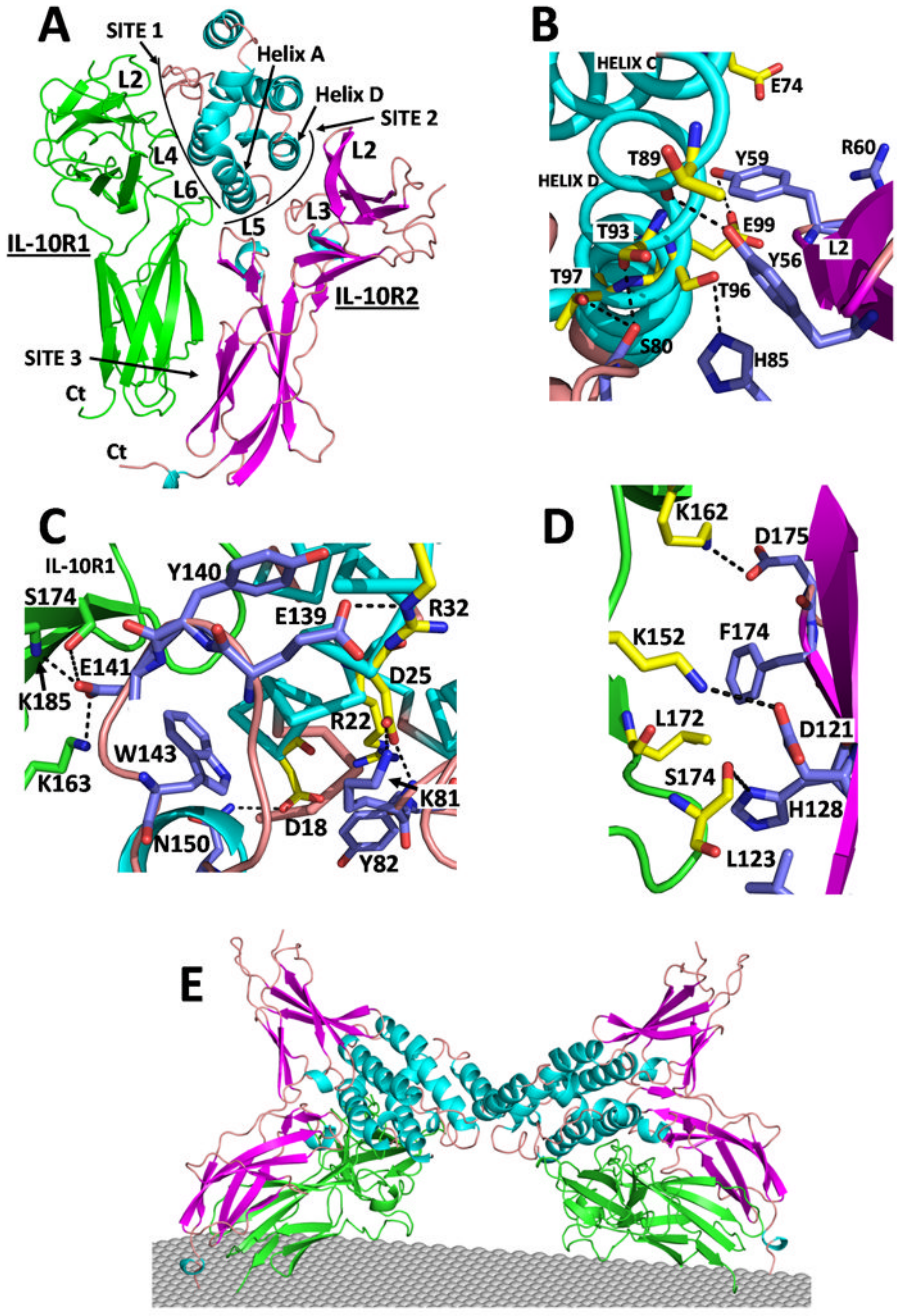

Figure 5. cmvIL-10 Ternary complex

(A) Overall structure of the cmvIL-10 ternary complex. **(B)** Site 2 interactions between helix D and the L2/L3 cleft. **(C)** Site 2 interactions between helix A and the L3/L5 cleft. **(D)** Site 3 contacts. **(E)** Dimeric cmvIL-10 signaling complex. (See also Figures S6 and Tables S1-S4).

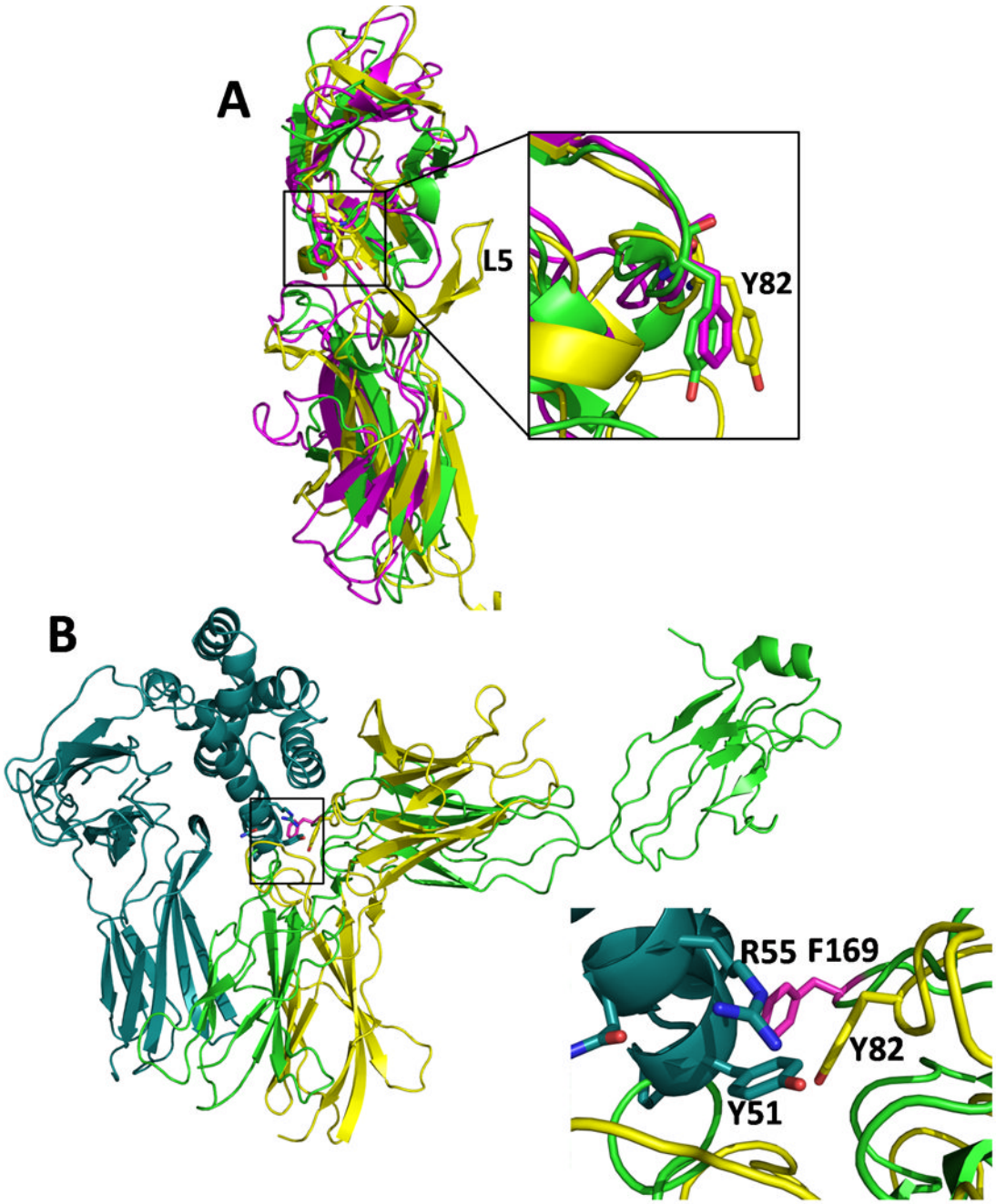

Figure 6. Common binding epitope identified between the promiscuous shared cytokine receptors

(A) Superposition of sIL-10R2 (yellow), gp130 (magenta), and γc chain (green). The inset shows the structural similarity of L3 loop residues $Y82^{sIL\text{-}10R2}$, $F169^{gp130}$ ($F191^{gp130}$ in uniprot database P40189), and $Y103^{\gamma c}$. EPOR and the growth hormone receptor (GHR) also have aromatic L3 residues ($F93^{EPOR}$ and $W104^{GHR}$) which have diverged from the structural alignment shown in Figure 6A (See Figure S7). **(B)** The position of $Y82^{sIL\text{-}10R2}$ and $F169^{gp130}$ are conserved in their respective ternary complexes. Ribbon diagram of the IL-22TC model (Fig 4) with IL-22/sIL-22R1 colored cyan and sIL-10R2 colored yellow. IL-6 from the IL-6/IL-6R/gp130 complex (pdbid 1P9M, (Boulanger et al., 2003)) was

superimposed onto IL-22 from the IL-22TC model (Fig 4) and the position of gp130 (green) is shown. The inset shows IL-22 residues $Y51^{IL\text{-}22}$, and $R55^{IL\text{-}22}$ along with $Y82^{sIL\text{-}10R2}$ (yellow) and $F169^{gp130}$ (magenta).

Table 1

sIL-10R2 Data Collection, Phasing, and Refinement Statistics

	Crystal 1	Crystal 2
Space group	P6	P6
Cell a,b	124.27	124.84
Cell c	83.70	84.22
Wavelength (Å)	0.97934 (peak)	1.00000
Resolution	50–2.5	50–2.14
Highest resolution	2.59–2.50	2.22–2.14
Completeness (%)	100 (100)	97.5 (84.6)
Redundancy	10.8 (10.7)	11.0 (5.1)
I/σ	72 (26)	50 (5.9)
R_{sym} (%)	7.1 (15.7)	7.1 (28.9)
Phasing statistics		
# Se (SOLVE)	12	
FOM (SOLVE)	0.48	
FOM (CNS DM)	0.91	
Refinement statistics		
Resolution (Å)		50–2.14
Highest resolution		2.14–2.16
R_{work} (%)		21.0 (27.7)
No. of reflections (work)		38,362
R_{free} (%)		23.9 (36.5)
No. of reflections (free)		2,016
Residues in model		A: 20–220
		B: 20–215
No. of protein atoms		3,284
No. of water atoms		212
No. of sulfate		10
No. of glycerol		1
Rmsd bond distance (Å)		0.0085
Rmsd bond angles (°)		1.43
Average B factor ($Å^2$)		37.3
Ramachandran plot		
Most favored (%)		88.1
Additionally allowed (%)		9.6
Generally allowed (%)		1.4
Disallowed (%)		0.8